Gas-Phase Detection of HSOH: Synthesis by Flash Vacuum Pyrolysis of Di-*tert*-butyl Sulfoxide and Rotational-Torsional Spectrum

Gisbert Winnewisser,*[a] Frank Lewen,[a] Sven Thorwirth,[a] Markus Behnke,[b] Josef Hahn,*[c] Jürgen Gauss,*[d] and Eric Herbst*[b]

Abstract: Gas-phase oxadisulfane (HSOH), the missing link between the well-known molecules hydrogen peroxide (HOOH) and disulfane (HSSH), was synthesized by flash vacuum pyrolysis of di-*tert*-butyl sulfoxide. Using mass spectrometry, the pyrolysis conditions have been optimized towards formation of HSOH. Microwave spectroscopic investigation of the pyrolysis products allowed—assisted by high-level quantum-chemical calculations—the first measurement of the rotational-torsional spectrum of HSOH. In total, we have measured approximately 600 lines of the rotational-torsional spectrum in the frequency range from 64 GHz to 1.9 THz and assigned some 470 of these to the rotational-torsional spectrum of HSOH in its ground torsional state. Some 120 out of the 600 lines arise from the isotopomer $H^{34}SOH$. The HSOH molecule displays strong *c*-type and somewhat weaker *b*-type transitions, indicating a nonplanar skew chain structure, similar to the analogous molecules HOOH and HSSH. The rotational constants (MHz) of the main isotopomer ($A = 202\,069$, $B = 15\,282$, $C = 14\,840$), determined by applying a least-squares analysis to the presently available data set, are in excellent agreement with those predicted by quantum-chemical calculations ($A = 202\,136$, $B = 15\,279$, $C = 14\,840$). Our theoretical treatment also derived the following barrier heights against internal rotation in HSOH (when in the *cis* and *trans* configurations) to be $V_{cis} \approx 2216\ cm^{-1}$ and $V_{trans} \approx 1579\ cm^{-1}$. The internal rotational motion results in detectable torsional splittings that are dependent on the angular momentum quantum numbers J and K_a.

Keywords: ab initio calculations · flash vacuum pyrolysis · mass spectrometry · oxasulfanes · rotational spectroscopy

Introduction

The well-studied molecules HOOH, hydrogen peroxide, and HSSH, disulfane, are known to have their equilibrium geometries in neither the *cis* nor the *trans* configuration, but to possess an equilibrium torsional angle η in between these two possibilities (113.7° for HOOH and 90.3° for HSSH), where $\eta = 0°$ and 180° refer to the *cis* and *trans* configurations, respectively.[1, 2] Indeed, potential barriers exist at both $\eta = 0°$ and 180°, and these affect the torsional motion and its interaction with the end-over-end rotation of the molecules. The net result is a splitting in the rotational spectrum as a function of the torsional state and, to a lesser extent, of the rotational quantum numbers. In the ground torsional state, the splitting seen for disulfane is rather small (< 100 kHz),[1] and not very dependent on rotational quantum numbers. The splitting seen for hydrogen peroxide is much larger (≈680 GHz) and depends more strongly on rotation.[3]

According to previous ab initio calculations,[4] as well as those reported here, the molecule HSOH, known as hydrogen thioperoxide or oxadisulfane, is a nonplanar molecule with a skew structure analogous to HOOH and HSSH. In Figure 1, we display the calculated structure of HSOH along with the experimentally determined "partial equilibrium" structures of HSSH and HOOH.[2, 5–7] To derive these "partial equilibrium structures", we have taken the ro-vibrational contributions of the torsional motion into account and removed them.[7] The HSOH bond lengths and angles fit smoothly into the geo-

[a] Prof. Dr. G. Winnewisser, Dr. F. Lewen, Dr. S. Thorwirth
I. Physikalisches Institut, Universität zu Köln
Zülpicher Strasse 77
50937 Köln (Germany)
Fax: (+49) 221-470-5162
E-mail: winnewisser@ph1.uni-koeln.de

[b] Prof. Dr. E. Herbst, Dr. M. Behnke
Departments of Physics and Astronomy, The Ohio State University
174 West 18th Avenue
Columbus, OH 43210 (USA)
Fax: (+1) 614-292-7557
E-mail: herbst@mps.ohio-state.edu

[c] Prof. Dr. J. Hahn
Institut für Anorganische Chemie, Universität zu Köln
Greinstrasse 6
50939 Köln (Germany)
Fax: (+49) 221-470-4899
E-mail: hahn@uni-koeln.de

[d] Prof. Dr. J. Gauss
Institut für Physikalische Chemie, Universität Mainz
55099 Mainz (Germany)
Fax: (+49) 6131-39-23895
E-mail: gauss@mail.uni-mainz.de

 DOI: 10.1002/chem.200305192

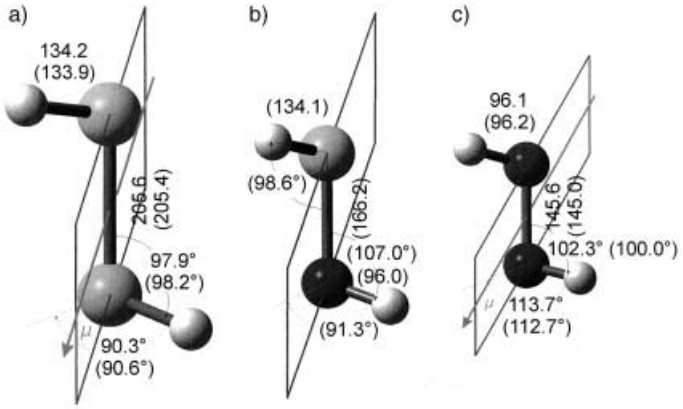

Figure 1. Comparison between the experimental and theoretical (in parentheses; CCSD(T)/cc-pCVQZ calculations, see text for details) geometrical structures of the three molecules a) HSSH, b) HSOH, and c) HOOH. Bond lengths given in pm. Planes shown bisect torsional angles. For HSSH and HOOH, the dipole moment μ lies in this plane.

metries displayed by the two "parent" molecules HOOH and HSSH.

Laboratory studies on HSOH are very sparse. The infrared spectrum of this molecule, produced by the photolysis of ozone (O_3) and hydrogen sulfide (H_2S), was previously detected in an argon matrix.[8] In addition, HSOH was generated from an H_2S/N_2O mixture in a chemical ionization source and detected in the neutralization – reionization (NR) arrangement of a four-sector mass spectrometer.[9]

Evidently none of the described synthetic routes is well suited to prepare larger quantities of HSOH, as is needed for its characterization by microwave spectroscopy. Thus, we chose to attempt a new synthesis of HSOH by flash vacuum pyrolysis (FVP) of di-*tert*-butyl sulfoxide. As seen from the synthesis of various organosulfenic acids RSOH by FVP of *tert*-butyl organo sulfoxides *t*BuS(O)R,[10] we expected the elimination of isobutene and the formation of *tert*-butylsulfenic acid as intermediate in the first step. Elimination of a second isobutene molecule via a four-membered transition state could then lead to the formation of HSOH [Eq. (1)].

To the best of our knowledge, this route has not been explored so far. However, its feasibility is indicated by the successful generation of HSSOH during the thermal decomposition of di-*tert*-butyldisulfane monoxide, *t*Bu-S(O)S-*t*Bu.[11]

In the present paper we describe the gas-phase synthesis of oxadisulfane based on the flash vacuum pyrolysis of di-*tert*-butyl sulfoxide. Details of our mass spectrometric analysis and optimization of the pyrolysis conditions are reported. This is followed by a section on high-level quantum-chemical calculations, as those turned out to be essential for the detection of HSOH by microwave spectroscopy. Finally, the rotational-torsional spectrum of HSOH is presented together with a discussion of its main spectroscopic features. The nature of the spectrum and the excellent agreement with theoretical predictions leave no doubt that HSOH has been synthesized and that its structure and torsional motion resemble, to a large extent, those of the analogous species HOOH and HSSH.

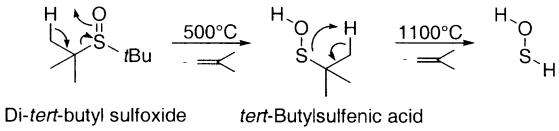

Di-*tert*-butyl sulfoxide *tert*-Butylsulfenic acid (1)

Results and Discussion

Pyrolysis of di-*tert*-butyl sulfoxide and mass spectrometric analysis of the pyrolysis products: Pyrolysis was carried out by passing di-*tert*-butyl sulfoxide at a constant flow rate and at a pressure of 2.2×10^{-3} mbar through a quartz tube heated by an oven. The temperature was increased in steps of 100 °C and the pyrolysis products were detected by using a quadrupole mass spectrometer (for details see Experimental Section). Before starting the heating cycle, the electron energy of the electron-ionization ion source was adjusted to a value (20 eV) where the signal of the molecular ion ($M^{+\bullet}$) was maximized relative to its fragmentation products for the spectrum at room temperature.

The mass spectrum of di-*tert*-butyl sulfoxide obtained at room temperature is shown in Figure 2. Since di-*tert*-butyl sulfoxide itself has not been the subject of a reported mass spectrometric investigation, and our instrumentation does not allow MS/MS experiments, our interpretation of the observed spectrum is based on the results obtained by Smakman and de Boer[12] for related aliphatic sulfoxides. They found that

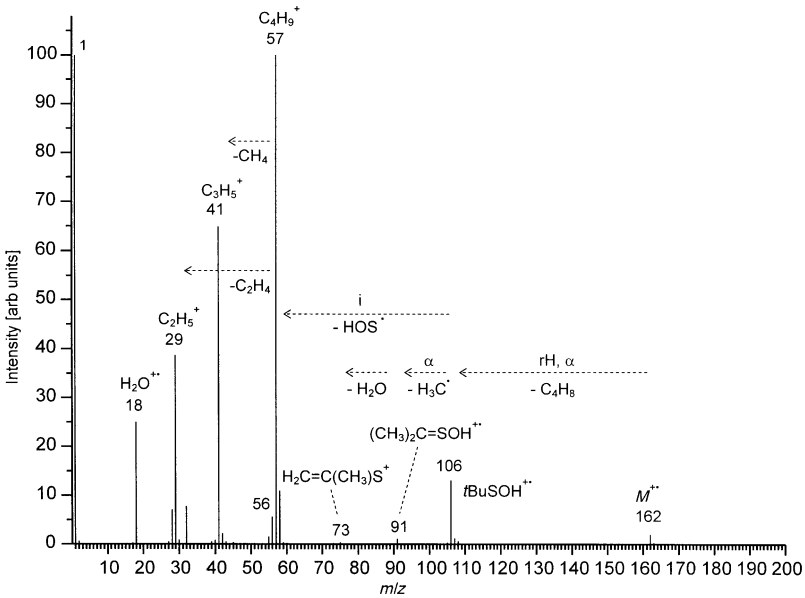

Figure 2. Observed fragmentation pattern in the mass spectrum of the precursor di-*tert*-butylsulfoxide at room temperature (quadrupole RGA, EI, 20 eV, enclosed ion source, $p = 2.2 \times 10^{-3}$ mbar).

increasing branching at the α-carbon atom of the sulfoxides strongly favors the elimination of an alkene moiety from the molecular ion by preferential fission of the higher substituted C–S bond. In the case of di-*tert*-butyl sulfoxide, this process would lead to the elimination of isobutene [Eq. (2)].

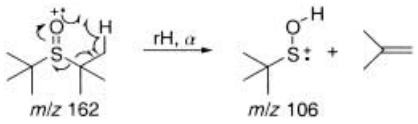

(2)

The resulting daughter ion tBuSOH$^{+\bullet}$ of this first fragmentation step can be seen as the parent ion of all other fragmentation reactions [Eqs. (3)–(5)].

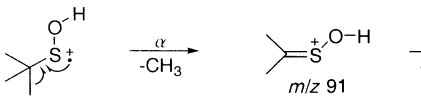

(3)

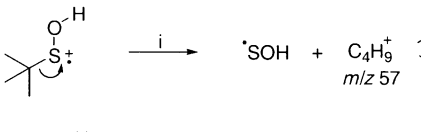

(4)

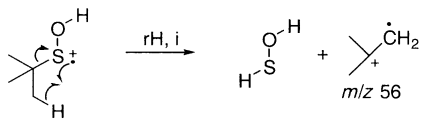

(5)

It cannot be excluded, however, that inductive cleavage of tBuSO$^{\bullet}$ from the $M^{+\bullet}$ ion also contributes to the formation of $C_4H_9^+$ (m/z 57, base peak of the spectrum).

There is no indication for the formation of the HSOH$^{+\bullet}$ ion (m/z 50) in the room-temperature spectrum. This situation changes when the temperature of the thermolysis tube is increased. The evolution of the mass spectrum with increasing pyrolytic temperature is presented in Figure 3. The onset of the thermal decomposition of di-*tert*-butyl sulfoxide is indicated by the strong increase of the signal at m/z 56 above 200 °C. Simultaneously, the intensity of the $M^{+\bullet}$ signal decreases, while the signal at m/z 106 remains constant. This observation corresponds to the expected thermal elimination of isobutene (m/z 56) and the formation of *tert*-butylsulfenic acid (m/z 106) in the first step of the thermolysis [Eq. (1)]. Evidently, the $M^{+\bullet}$ ions of the pyrolysis products ($C_4H_8^{+\bullet}$ and $C_4H_{10}SO^{+\bullet}$) cannot be distinguished from the analogous fragment ions of tBu$_2$SO$^{+\bullet}$ so that the corresponding peaks are superimposed in the spectrum.

The decomposition of tBuSOH begins at 500 °C and is indicated by the decrease in intensity of the signal at m/z 106, and a further increase of the $C_4H_8^{+\bullet}$ signal. At that temperature, the $M^{+\bullet}$ ion of di-*tert*-butyl sulfoxide has completely vanished, indicating its complete thermal decomposition in the pyrolysis zone. Thus, the further increase of the $C_4H_8^{+\bullet}$ signal refers to an isobutene elimination from tBuSOH. Concomitantly with the decomposition of tBuSOH, two new signals appear in the spectrum at m/z 48 and m/z 50. Since there are no further reasonable isobaric species (i.e. the formation of CH_3SH and O_3 (m/z 48) or C_4H_2 and H_2O_3 (m/z 50) can be excluded under the given conditions), the new signals were assigned to SO and HSOH, respectively. Thus, the mass spectra obtained at temperatures above 500 °C are most compatible with the thermal decomposition of tBuSOH to form isobutene and oxadisulfane.

Since HSOH$^{+\bullet}$ has not been observed as a fragmentation product of tBu$_2$SO$^{+\bullet}$, and since it therefore cannot be a fragment ion of tBuSOH$^{+\bullet}$, it is most probably generated by the ionization of the gas-phase species HSOH. To further characterize the origin of the HSOH$^{+\bullet}$ peak, the spectra of the pyrolysis products formed at 1100 °C were measured at different ionization energies. With decreasing ionization energy, one would expect an increase of the relative intensities of molecular ions with respect to the intensities of the fragment ions (Figure 4). At that temperature, isobutene is the most abundant pyrolysis product. Therefore, the spectrum is dominated by the signals of the molecular ion $C_4H_8^{+\bullet}$ and its fragment ions m/z 41 ($M^{+\bullet}$ – $H_3C^{\bullet}$) and m/z 28 ($M^{+\bullet}$ – C_2H_4). Additional relatively stable species that could be formed during pyrolysis must formally be derived from HSOH. Thus, beside the strong peak of $H_2O^{+\bullet}$ at m/z 18, additional weak peaks were assigned as follows: m/z 2 to $H_2^{+\bullet}$, m/z 32 to $S^{+\bullet}$, m/z 34 to $H_2S^{+\bullet}$, m/z 64 to $SO_2^{+\bullet}$ and/or $S_2^{+\bullet}$, m/z 80 to $S_2O^{+\bullet}$ ($SO_3^{+\bullet}$ is less probable).

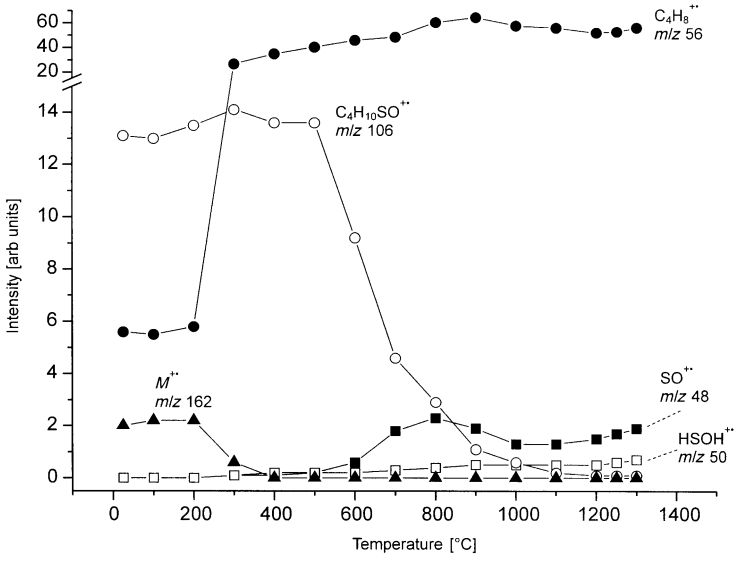

Figure 3. Evolution of the pyrolysis reaction products of di-*tert*-butyl sulfoxide monitored by mass spectrometry (quadrupole RGA, EI, 20 eV, enclosed ion source, $p = 2.2 \times 10^{-3}$ mbar).

When the ionization energy is diminished from 20 to 15 eV, the overall ion yield becomes smaller by approximately one order of magnitude (Figure 4).

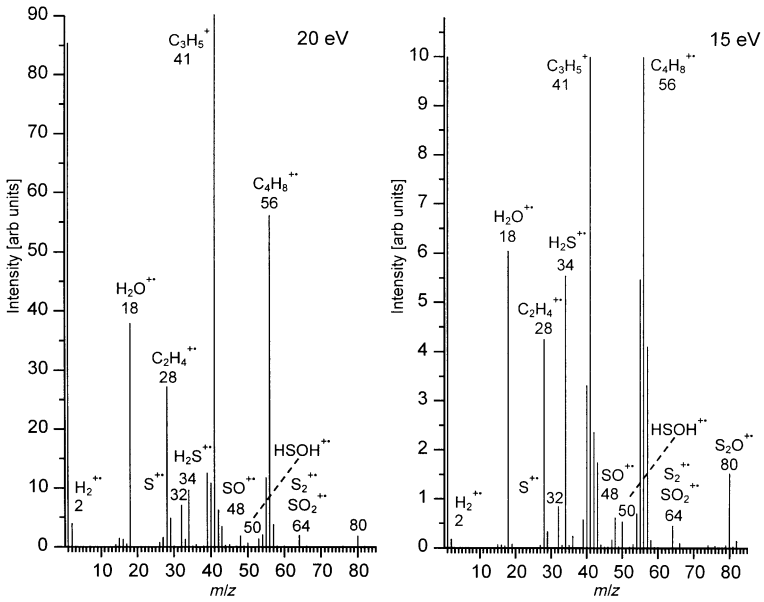

Figure 4. Mass spectra of HSOH resulting from the flash vacuum pyrolysis reaction of di-*tert*-butylsulfoxide at 1100 °C. The spectra are recorded at two different ionization energies in order to distinguish between fragmentation ions and molecular ions (quadrupole RGA, EI, 20 eV and 15 eV, enclosed ion source, $p = 2.2 \times 10^{-3}$ mbar). No signals were observed above *m*/*z* 85.

A comparison of the relative signal intensities in the two spectra reveals clear differences. The intensities of the peaks at *m*/*z* 18, 34, 50, and 80 clearly become stronger with respect to the signals found at *m*/*z* 32, 48, and 64. This leads to the assumption that $H_2O^{+\bullet}$, $H_2S^{+\bullet}$, $HSOH^{+\bullet}$, and $S_2O^{+\bullet}$ are formed by the ionization of the corresponding molecular species, whereas the other peaks correspond to fragment ions: $S^{+\bullet}$ is probably generated from $H_2S^{+\bullet}$, $SO^{+\bullet}$ from $HSOH^{+\bullet}$ and/or $S_2O^{+\bullet}$, and $S_2^{+\bullet}$ (SO_2 should rather correspond to a molecular ion) from $S_2O^{+\bullet}$. A special situation arises for the signal at *m*/*z* 2 that has been assigned to $H_2^{+\bullet}$. One might argue that many multipole devices do not work properly at low masses and switch to full transmission instead. By recording spectra on different suitable organic samples (e.g. perfluorotributylamine (PFTBA)) we were able to prove that only *m*/*z* 1 is significantly affected by this interference while in all cases ion intensities for *m*/*z* 2 were found to be below 0.5 % of the base peak. We therefore assume that, in spite of its intensity decrease, the $H_2^{+\bullet}$ peak indicates the presence of molecular hydrogen in the pyrolysis gas. Its decrease in relative intensity in the low-energy mass spectrum must be attributed to the extraordinarily high ionization energy of the hydrogen molecule (15.4 eV).[13]

The formation of molecular hydrogen can be explained by the decomposition of oxadisulfane. By analogy with the well-known condensation reaction of organo sulfenic acids,[14] sulfenic acid itself most probably reacts via condensation of water to form disulfane monoxide [Eq. (6)].

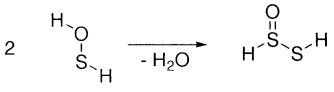

(6)

It can be assumed that this unstable primary condensation product quickly decomposes into H_2 and S_2O. Since, at the given pressure of 2.2×10^{-3} mbar, intermolecular collisions are much less frequent than collisions with the wall, the decomposition reaction most probably takes place on the glass wall of the spectrometer cell.

Quantum-chemical calculations: Quantum-chemical calculations can be used to predict the HSOH rotational-torsional spectrum and to derive parameters that can be compared with those obtainable from the experimental spectrum. The three rotational constants A_0, B_0, and C_0 belonging to the ground vibrational state, the size of the permanent electric dipole-moment vector $\boldsymbol{\mu}$ and its components μ_a, μ_b, and μ_c along the three principal axes *a*, *b*, and *c*, and the two torsional barriers V_{cis} and V_{trans} were of most interest.

Despite impressive progress in the accuracy achieved by present-day ab initio calculations, the reliable prediction of a rotational spectrum remains a very challenging task. The quality of the derived rotational constants critically depends on the level of accuracy of the calculated equilibrium geometry of the molecule. It is well established that an accurate determination of the geometrical parameters requires explicit inclusion of electron correlation.[15] Benchmark calculations have demonstrated that the coupled-cluster (CC) approach[16] and, in particular, the coupled-cluster singles and doubles (CCSD) model augmented by a perturbative treatment of triple excitations (CCSD(T))[17] are capable of providing highly accurate geometrical parameters, provided sufficiently large basis sets are used.[15] For compounds with first-row elements only, it has been shown that CCSD(T) calculations with a correlation-consistent polarized valence quadruple-zeta basis set (e.g., the cc-pVQZ set)[18] will yield *equilibrium* bond lengths with an accuracy of approximately 0.002 to 0.003 Å, and bond angles with an accuracy of approximately 0.1 degrees.[15] To obtain the same accuracy for molecules involving second-row elements—as is the case for HSOH—is a more challenging task. It seems to be achievable by using the corresponding polarized core-valence basis sets (e.g., cc-pCVQZ)[18] to ensure an adequate inner-shell description.[19]

Calculations were performed at the second-order Møller–Plesset perturbation (MP2) level of theory[20] as well as at the coupled-cluster singles and doubles (CCSD) level[21] augmented by a perturbative treatment of triple excitations (CCSD(T))[17] using basis sets taken from Dunning's hierarchy of correlation-consistent basis sets (i.e., cc-pVTZ, cc-pVQZ, and cc-pCVQZ).[18, 22] Equilibrium geometries, as

well as the corresponding rotational constants, have thus been obtained at the MP2/cc-pVTZ, CCSD(T)/cc-pVTZ, CCSD(T)/cc-pVQZ, and CCSD(T)/cc-pCVQZ levels using analytical energy gradients.[23]

To obtain accurate rotational constants, vibrational corrections have to be considered, since the vibrationally averaged constants A_0, B_0, and C_0 and not the equilibrium values A_e, B_e, and C_e are the relevant parameters for the simulation of the rotational spectra. Based on a perturbational treatment starting from the harmonic oscillator rigid-rotator approximation, these corrections are obtained for the vibrational ground state in the form [Eq. (7)],

$$B_0 = B_e - \frac{1}{2}\sum_r \alpha_r \qquad (7)$$

where the α_r values are the vibration–rotation interaction constants, and the sum is over all normal modes r. The calculation for each α_r value involves three contributions.[24, 25] The first accounts for the quadratic dependence of B on the normal coordinates Q_r; the second is due to Coriolis interactions between different normal modes; the third arises from anharmonic contributions to the expectation values of the normal coordinates Q_r. The first two terms are easily obtained from an available harmonic force field, while the third term requires computation of parts of the cubic force and thus is the computationally most expensive step. The vibrational corrections have been computed at the MP2/cc-pVTZ and CCSD(T)/cc-pVTZ levels. For this purpose the required harmonic force fields have been computed by using analytic second-derivative techniques,[24, 25] while the corresponding cubic force fields have been obtained by means of finite difference techniques with displacements taken along the normal coordinates as described, for example, in reference [26]. All reported calculations have been carried out using the Mainz–Austin version of the ACESII program package.[27]

Table 1 summarizes the geometrical parameters, equilibrium rotational constants A_e, B_e, and C_e, and the vibrationally corrected ground-state rotational constants A_0, B_0, and C_0 obtained for $H^{32}SOH$ at various theoretical levels, that is, from MP2/cc-pVTZ to CCSD(T)/cc-pCVQZ with increasing reliability. The changes in the rotational constants, when going from CCSD(T)/cc-pVQZ to CCSD(T)/cc-pCVQZ, are smaller than 1 %, but still amount to more than 500 MHz for A_e and up to 100 MHz for B_e and C_e. Conservatively estimated, the accuracy for the equilibrium values can be quoted to be approximately 500 MHz for the A constant and 100 MHz for the B and C rotational constants.

Table 1. Geometrical parameters (distances in Å, angles in degrees), rotational constants [MHz], and dipole moments [D] for $H^{32}SOH$ calculated at various theoretical levels.

	MP2/ cc-pVTZ	CCSD(T)/ cc-pVTZ	CCSD(T)/ cc-pVQZ	CCSD(T)/ cc-pCVQZ
a) Geometrical parameters				
R(SO)	1.6722	1.6772	1.6677	1.6619
R(SH)	1.3385	1.3442	1.3435	1.3414
R(OH)	0.9618	0.9607	0.9592	0.9601
α(OSH)	98.43	98.34	98.40	98.55
α(SOH)	105.82	105.97	106.87	107.01
τ(HSOH)	91.40	91.42	91.38	91.29
b) Rotational constants				
A_e	202939.9	201934.7	203009.2	203567.7
B_e	15236.6	15150.1	15301.2	15397.6
C_e	14832.9	14742.8	14882.3	14976.7
A_0	201641.6	200502.8	201577.3[a]	202135.8[a]
B_0	15119.3	15031.4	15182.5[a]	15278.9[a]
C_0	14699.3	14606.5	14746.0[a]	14840.4[a]
c) Dipole moment components				
μ_a	0.0435	0.0544	0.0182	0.0441
μ_b	0.8030	0.7731	0.7682	0.7729
μ_c	1.4808	1.4644	1.4321	1.4329

[a] Using vibrational corrections computed at the CCSD(T)/cc-pVTZ level.

The rotational constants A_0, B_0, and C_0 for the ground vibrational state differ from their equilibrium values by 1300 to 1500 MHz for the A constant and by 100 to 150 MHz for the B and C constants. The residual error in the predicted rotational constants is estimated to approximately 500 MHz for A_0 and 100 MHz for B_0 and C_0. However, as will be seen later, the comparison between theoretically calculated and experimentally obtained rotational constants turns out to be considerably more favorable for HSOH than the theoretically estimated uncertainties suggest.

Dipole-moment components computed at different theoretical levels are also given in Table 1. These are needed for the theoretical prediction of the rotational spectrum and the intensities of the lines. The torsional barrier heights for HSOH calculated in this study are presented in Table 2 together with experimentally and theoretically determined barrier heights for HSSH and HOOH.[28] Inspection of Table 2 reveals that the *cis* barrier for HSOH is considerably higher than that for HOOH, but lower than that for HSSH. A more detailed discussion will be presented in a forthcoming paper.

Table 2. Barrier heights [cm^{-1}] for *cis* and *trans* configurations of HOOH, HSSH, and HSOH.

Species	Theory[a]		Experiment[b]	
	V_{cis}	V_{trans}	V_{cis}	V_{trans}
HSSH	2791	2016	2843	2037
HSOH	2216	1579	–	–
HOOH	2552	372	2562.8	387.07

[a] Present calculations (CCSD(T)/cc-pCVQZ level). [b] See ref. [28].

Rotational-torsional spectrum of HSOH: The search for HSOH among the pyrolytic products of tBu$_2$SO and the analysis of its experimental spectrum were greatly aided by the quantum-chemical calculations discussed above and by knowledge of the expected prominent spectral features. Because of its nearly right-angle chain structure, HSOH, like HOOH and HSSH, is an asymmetric top molecule close to the limit of a prolate symmetric top, in which the B and C rotational constants are equal but less than the A constant. For HSOH, the corresponding a principal axis lies nearly parallel to the chain axis, while the b and c axes lie nearly perpendicular to the chain. The small inertial asymmetry arises from the special mass distribution associated with the chain structure of the molecules. The asymmetry can be expressed quantitatively by Ray's asymmetry parameter $\kappa = (2B - A - C)/(A - C)$, which is -1 for the case of a prolate symmetric top. According to our quantum-chemical calculations, κ is -0.993 for H^{32}SOH.

The rotational levels of an asymmetric top are labeled by the total angular-momentum quantum number J, and by the pseudo-quantum numbers K_a and K_c, which represent the projection of the angular momentum on the a and c principal axes.[29] For a near prolate symmetric top, one often refers to K_a as K, the actual projection quantum number in the prolate limit. The HSOH molecule can be expected to display a spectrum with extremely weak a-type transitions ($\Delta K_a = 0, \pm 2$; $\Delta K_c = \pm 1, \pm 3$) and a dominating perpendicular-type spectrum with strong c-type ($\Delta K_a = \pm 1, \pm 3$; $\Delta K_c = 0, \pm 2$) and somewhat weaker accompanying b-type ($\Delta K_a = \pm 1, \pm 3$; $\Delta K_c = \pm 1, \pm 3$) transitions, as can be understood from the theoretical values (Table 1) of the dipole-moment components μ_a, μ_b, and μ_c. Due to the small value of μ_a, which is roughly aligned to the SO bond, no a-type transitions have been observed in the present investigation. The HSOH spectrum consists of regularly spaced compact Q branches consisting of sets of $\Delta J = 0$ transitions, and easily discernable P ($\Delta J = -1$) and R ($\Delta J = +1$) branches that are spread out over wider frequency ranges. The Q branches are characterized by a notation such as $^rQ_1$, where the Q stands for transitions with $\Delta J = 0$, the superscript r for transitions which increase K_a by one, and the subscript 1 for the K_a value of the lower energy level in all transitions of the band, which is 1 in this case. For K_a different from zero, two sub-branches exist, according to the values of K_c, which are split because of inertial asymmetry. The transition with the lowest allowable J is referred to as the origin. Note that this notation makes no distinction between c-type and b-type transitions, so that in a species such as HSOH, with both b-type and c-type transitions, there is a doubling in the number of sub-branches.

A broad overview of the pattern of P, Q, and R branches is best obtained with the aid of a Fortrat diagram, shown in Figure 5 for HSOH. In this diagram, where frequency is the abscissa and the quantum number J', referring to the upper energy level, the ordinate, the grouping of individually measured transitions into branches and sub-branches stands out. In particular, one can see the location of the branch origins, or transitions with lowest J' values, for the $^rQ_0$, $^rQ_1$, and $^rQ_2$ branches, and the J' dependence of the sub-branches, resulting in increasing splitting as J' increases. The origins are found approximately at frequencies of $(A - B)$ $(2K_a + 1)$, where K_a assumes the values 0, 1, 2,... According to our quantum-chemical calculations, the $K_a = 1 - 0$ band origin should occur at 187 GHz, exactly where it is observed. Moreover, the frequency spacing between c-type and b-type lines for each J' in the $^rQ_0$ branch is determined to be first order by the difference $1/2(C - B)J'(J' + 1)$; $(C - B)$ has been determined experimentally to be -442 MHz, very close to the theoretically predicted value of -439 MHz.

For the first detection of HSOH we used the frequency region of the $^rQ_1$ branch ($\Delta J = 0$; $K_a = 2 - 1$), with its origin near 560 GHz. In Figure 6, we present a series of sample spectra recorded when HSOH was first observed. It is evident that each c-type transition appears as a doublet split by about 18 MHz. This unmistakable internal rotation pattern, which arises from opposite changes in torsional substates during c-type rotational transitions,[1] was used as a first guide in the assignment of the dense line spectrum. Torsional splittings were observed for all transitions in HSOH and found to be strongly K_a-dependent. Within a K_a stack, the torsional splitting associated with K_a shows a somewhat weaker dependence on J. The occurrence and analysis of the internal rotation splittings will be discussed in detail in a separate publication.

Comparison of related species: Before the present study was started, all of the important characteristics of the expected perpendicular spectrum were worked out theoretically and experimentally, in analogy to the symmetric molecules HSSH

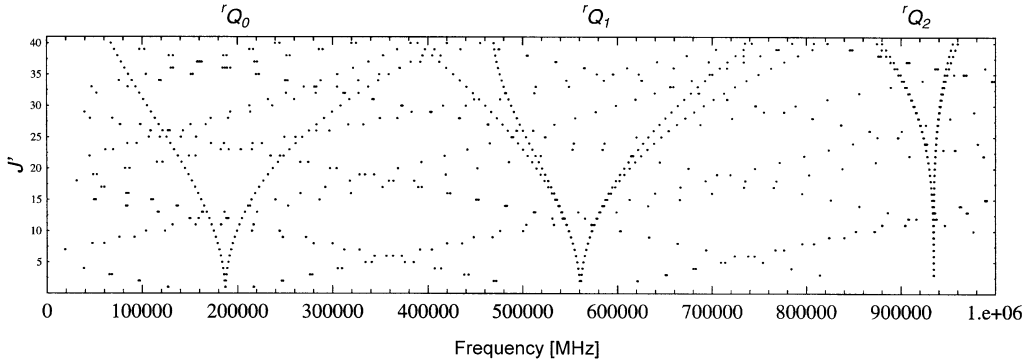

Figure 5. The Fortrat diagram for the vibrational ground state of HSOH. The rotational-torsional spectrum is depicted up to 1 THz. The observed torsional splittings are too small to be shown in this graph. The three Q branches labeled $^rQ_0$, $^rQ_1$, and $^rQ_2$ constitute the dominant features of this frequency range.

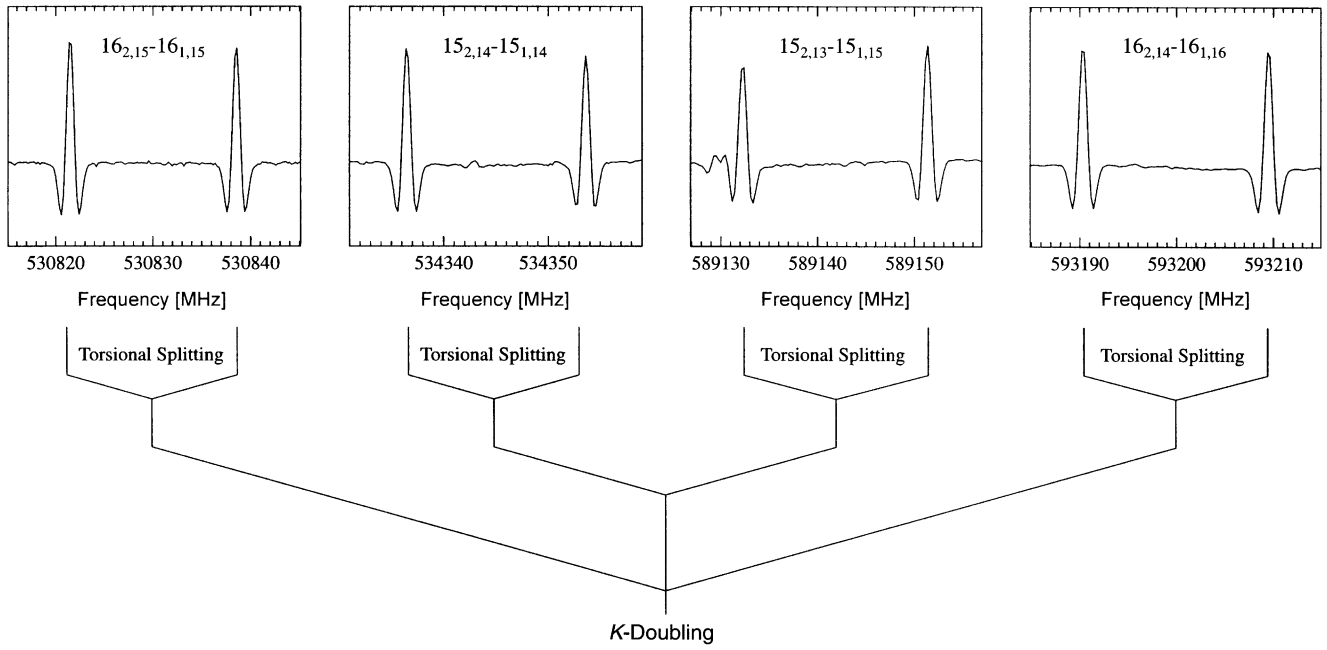

Figure 6. First detection of gas-phase H^{32}SOH near 561 GHz by means of the $^{r}Q_1$ branch. The traces present a series of individual J transitions recorded in such a fashion as to display the torsional splitting of the c-type transitions individually. The K doubling refers to the separation between levels characterized by the same K_a but different K_c.

and DSSD and their various nonsymmetric isotopomers such as HSSD, DS^{34}SD, HS^{34}SH. A marked difference exists between the two sets of species. The symmetric species HSSH and DSSD possess a C_2-symmetry axis which bisects the torsional angle.[1] The permanent electric dipole-moment vector $\boldsymbol{\mu}$ of the symmetric species is aligned along the C_2-symmetry axis.[1] Depending on the mass distribution expressed in terms of the moment of inertia tensor, the symmetric species display only c-type or only b-type spectra, since the symmetry axis lies along one of these two principal axes. The spectra of HSSH and DSSD exhibit c-type spectra only, and these display line-intensity alternations due to nuclear spin statistics, Fermi – Dirac in the former and Bose – Einstein in the latter.[30]

Substitution of an S atom for an O atom in one of the center positions to form HSOH destroys the C_2-symmetry axis and allows dipole-moment components along all three principal axes. With the missing symmetry, HSOH does not show any effects of intensity alternation of rotational lines. Figure 7 displays the calculated stick spectrum of the b-type and c-type sub-branches of the $^{r}Q_0$ branch of HSOH, which shows only a gradual change in intensity. This figure also displays four original recordings with two c-type and two b-type transitions, split due to torsional effects.

Determination of the molecular constants: A fit of all lines (470 for H^{32}SOH and 120 for H^{34}SOH) was achieved by using Pickett's program SPFIT, employing a Watson – Hamiltonian in the S reduction.[31] To account for torsional splitting and interaction of the torsional substates, a two-state fit was used. This fit was successful for all but the lines with highest K_a (4 – 5). These lines, weighed down in the current fit, will require a better treatment of the torsional motion. In addition to the various rotational and centrifugal distortion constants, the set of parameters consists of an energy difference between torsional substates ΔE and several J- and K-dependent Coriolis interaction parameters G_a. All determined parameters for H^{32}SOH as well as for H^{34}SOH are shown in Table 3. Rather than tabulating both lower and upper torsional state constants, we tabulate the average constants and half the differences between the values for the two states. The lines have been fit to a unitless root mean-square deviation of less than unity, indicating a fit to experimental accuracy. The average rotational constants determined and the highest-level calculated values given in Table 1 are in excellent agreement. In particular, the differences between the experimental and theoretical rotational constants for H^{32}SOH are only 67 MHz, 3 MHz, and 0.2 MHz for A, B, and C, respectively.[32]

Conclusion

Using the flash vacuum pyrolysis of di-*tert*-butyl sulfoxide, we have succeeded in developing a gas-phase synthesis for oxadisulfane (HSOH), the first member in the series of the oxoacids of sulfur and the heretofore missing link between disulfane and hydrogen peroxide. The new synthetic pathway led us to the unequivocal detection and assignment of the pure rotational spectrum of gas-phase HSOH in the frequency region between 64 GHz and 1.9 THz. This first detection of HSOH at the Cologne laboratory—after 15 years of trial and error—was made possible by the detailed predictions of the theoretical chemistry group at Mainz and the synthetic chemical techniques of the inorganic chemistry group at Cologne.

Using a quadrupole mass spectrometer, we were able to monitor the reaction products in the vacuum pyrolysis of di-

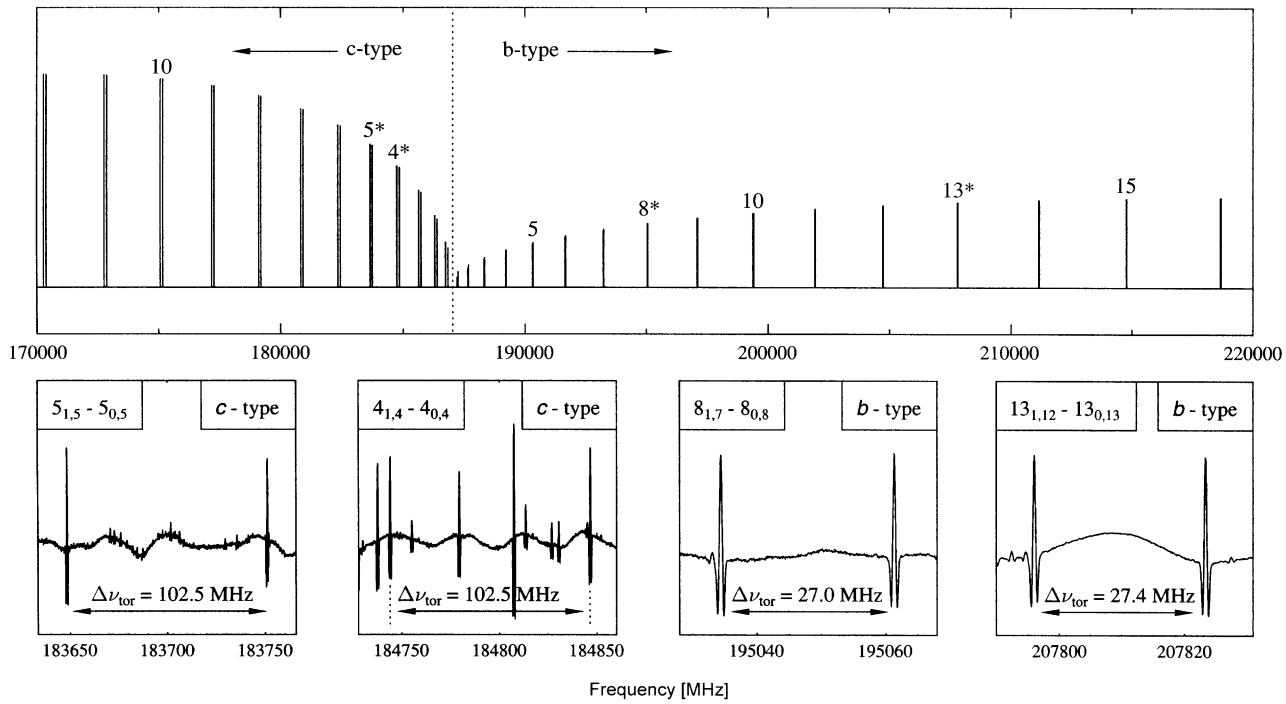

Figure 7. Stick spectrum of the $^{r}Q_0$ branch of $H^{32}SOH$. The branch exhibits fairly strong *c*-type and weaker *b*-type transitions. Note that no intensity alternation occurs. Individual actual transitions (marked by asterisks in the upper stick spectrum) are shown with their torsional splittings.

Table 3. Spectroscopic parameters for ground state $H^{32}SOH$ and $H^{34}SOH$ [MHz].[a]

Parameter	$H^{32}SOH$	$H^{34}SOH$
A	202 069.05431(134)	201 739.7641(129)
$\Delta A/2$	– 14.3805(39)	– 14.0255(139)
B	15 281.956620(123)	15 001.43940(38)
$\Delta B/2 \times 10^3$	– 2.7622(135)	– 2.686(89)
C	14 840.216440(121)	14 573.77816(39)
$\Delta C/2 \times 10^3$	4.3548(77)	4.155(38)
$D_J \times 10^3$	24.528463(138)	23.690720(304)
$\Delta D_J/2 \times 10^6$	0.3786(53)	0.266(44)
D_{JK}	0.3904340(48)	0.3787713(163)
$\Delta D_{JK}/2 \times 10^3$	0.2970(55)	0.3125(139)
D_K	5.989715(202)	5.97102(211)
$\Delta D_K/2$	– 1.07594(139)	– 0.79910(279)
$d_1 \times 10^3$	– 0.7161682(196)	– 0.681897(51)
$\Delta d_1/2 \times 10^6$	– 0.0220(35)	– 0.041(37)
$d_2 \times 10^3$	0.2911054(104)	0.270603(86)
$\Delta d_2/2 \times 10^6$	0.2907(52)	
$H_J \times 10^6$	– 0.015109(38)	– 0.014
$H_{JK} \times 10^6$	– 1.1950(39)	– 1.2
$\Delta H_{JK}/2 \times 10^6$	0.0565(33)	– 0.05
$H_{KJ} \times 10^3$	0.02987(32)	0.03
$\Delta H_{KJ}/2 \times 10^3$	0.01297(72)	0.014
$H_K \times 10^3$	0.6042(114)	0.6567
$\Delta H_K/2$	– 0.031089(203)	0.0227
$h_1 \times 10^9$	1.0178(79)	1.00
$h_2 \times 10^9$	– 1.5560(82)	– 1.50
$h_3 \times 10^9$	– 0.9528(209)	– 0.90
$\Delta L_K/2 \times 10^3$	0.3717(112)	
ΔE	64.5051(63)	64.1870(291)
G_a	– 32.786(42)	– 12.0193(270)
G_{aK}	6.1807(154)	
$G_{aJK} \times 10^3$	0.0705(79)	
G_{aKK}	– 0.24569(119)	
$G_{aJ} \times 10^3$	– 0.645(78)	

[a] Numbers in parentheses represent one standard deviation in terms of the least significant figures. No number indicates that the parameter was fixed at the value shown.

tert-butyl sulfoxide at different temperatures. Up to 500 °C, the formation of *tert*-butylsulfenic acid by isobutene elimination dominates the reaction. Increasing the pyrolysis temperature from 500 to 1100 °C leads to the formation of HSOH by isobutene elimination from the intermediate sulfenic acid.

Because the pyrolysis of di-*tert*-butyl sulfoxide is performed under continuous-flow conditions, it is well suited to maintain a constant HSOH concentration in a large volume gas cell as is needed for microwave spectroscopic characterization. Thus, following a mass spectrometric optimization of the pyrolysis, we were able to obtain the rotational-torsional spectrum of HSOH, assisted by high-level quantum chemical predictions of the rotational constants.

The HSOH molecule displays a clear-cut perpendicular-type spectrum, with strong *c*-type and weaker *b*-type transitions, indicating that HSOH possesses a nonplanar skew chain structure similar to HSSH and HOOH. Each transition of HSOH is split by the torsional motion that occurs between the two halves of the molecule, the OH and the SH bars. At the moment, we have measured approximately 600 transitions, of which 470 lines belong to the main isotopomer $H^{32}SOH$ and 120 lines to $H^{34}SOH$. All transitions belong to the ground torsional state.

To derive a reliable experimental structure from the observed spectra, the rotational constants of the different isotopomers have to be known. In addition to our studies of $H^{32}SOH$ and $H^{34}SOH$, we have recently succeeded in generating the perdeuterated isotopomer $D^{32}SOD$ by an rf-discharge of D_2O and D_2S. The spectral analysis of this species and the structural determination of oxadisulfane will be described elsewhere.[38]

Experimental Section

Di-*tert*-butyl sulfoxide: The precursor di-*tert*-butyl sulfoxide was prepared by selective oxidation of di-*tert*-butyl sulfide with hydrogen peroxide/selenium dioxide, as described by Drabowicz and Mikolajczyk.[33]

Pyrolysis arrangement: The flash vacuum pyrolysis (FVP) of di-*tert*-butyl sulfoxide was achieved by evaporating and passing this compound in vacuum through a quartz tube (inner diameter 1 cm, length 10 cm) heated by an oven with a thermocouple temperature controller. The pyrolysis apparatus was evacuated using a two-stage rotary vane pump and a liquid nitrogen cold trap, allowing pressures down to 5×10^{-4} mbar to be reached (Figure 8). All investigations were performed under flow conditions. A valve placed on top of the precursor reservoir flask controlled the flow rate of the precursor molecules into the system. The resulting pressure was monitored by using a Pirani gauge, which allowed only a certain amount of di-*tert*-butyl sulfoxide to evaporate into the heated quartz tube.

Mass-spectrometric instrumentation: The mass spectrometer employed a residual gas analyzer system (Microvision Plus (LM70), Leda-Mass Ltd., UK). The system consisted of an enclosed electron-ionization ion source in a cross-beam arrangement, with quadrupole analyzer 300D and channel plate detector. All parts of the spectrometer were kept in a separate case, including a turbo molecular pump to provide the operating pressure of 1×10^{-7} mbar for the quadrupole analyzer. The low-vacuum side of the turbo pump was flushed with purge gas (N_2) to keep the bearings clear of corrosive gases. A diaphragm pump was used as a roughing pump. A butterfly valve was used to separate the mass spectrometer from the system between data acquisition intervals in order to minimize contamination of the instrument. The chosen geometry (Figure 8) resulted in a distance of 15 cm between ion source and pyrolysis zone.

In order to analyze the decomposition products of di-*tert*-butyl sulfoxide in the vacuum pyrolysis, spectra were taken at various temperatures of the quartz tube (temperature range 25 °C – 1300 °C) at electron energies of the ion source between 15 and 20 eV and a pressure of 2.0×10^{-3} mbar. Under these conditions, the pressure in the analyzer region of the mass spectrometer was around 1×10^{-6} mbar.

Rotational spectroscopic instrumentation: Two absorption cells with Teflon windows, one 1 m in length with an inner diameter of 5 cm, and the other 2 m in length with an inner diameter of 10 cm, were used. The previously described oven with a quartz tube was attached at an angle of 90 degrees to one side of the absorption cells. The previously used quadrupole mass spectrometer was attached via a butterfly valve to the cell, and the decomposition of the precursor di-*tert*-butyl sulfoxide was monitored while the production rate of HSOH was optimized. Valves attached to the sample inlet and to the rotor vacuum pump were used to control the flow through the absorption cell. All spectroscopic data were taken under flow conditions, typically at a pressure of 2×10^{-2} mbar. By measuring the decay of the intensity of HSOH spectral lines, we were able to estimate a 1/e lifetime of ≈5 s under the conditions of our experiment. Figure 9 shows the measured decay of the intensity as a function of time.

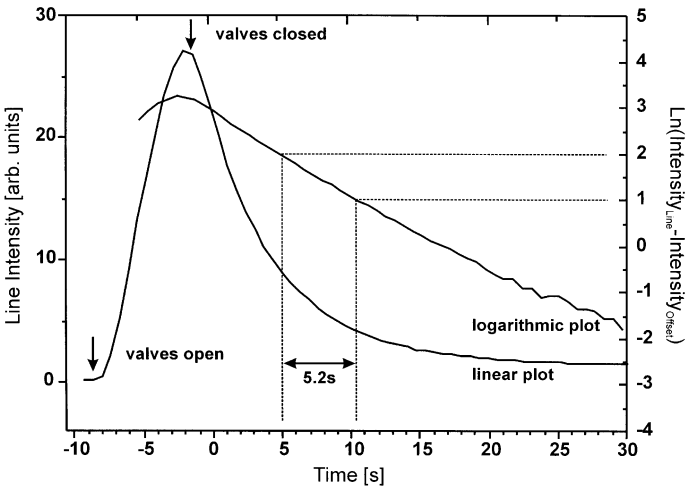

Figure 9. Measured decay of HSOH in a 2 m Pyrex absorption cell. A logarithmic plot of the decay demonstrates the expected exponential behavior.

The investigation of the spectra reported here covers a frequency region from about 64 GHz to 1900 GHz, a frequency span that cannot be achieved by one single spectrometer. Hence, several techniques have been employed to cover this large spectral range. In the regime from 64 – 178 GHz, a commercial spectrometer was used,[34] while radiation in the shorter millimeter-wave regime from 180 – 208 GHz was generated by employing a commercial 4 mm-wave synthesizer in connection with a planar Schottky Diode Multiplier[35] to make use of the third harmonic of the fundamental. The majority of lines were measured in the frequency region from 480 – 945 GHz by employing the Cologne Terahertz Spectrometer.[36] Finally, lines at 1800 – 1900 GHz were recorded with the Cologne Sideband Spectrometer for Terahertz Applications (COSSTA).[37] Magnetically tuned and liquid-helium cooled InSb bolometers were used as detectors.

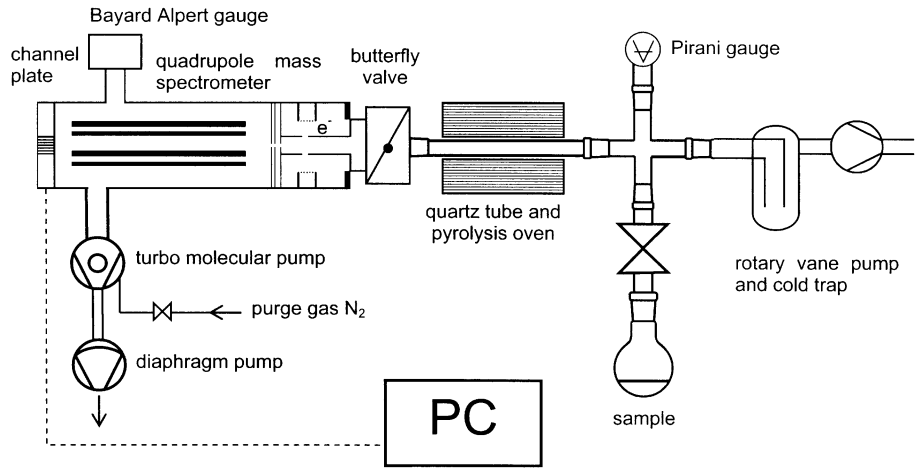

Figure 8. Flash vacuum pyrolysis arrangement with a mass spectrometer attached for initial diagnosis of the reaction products.

Acknowledgement

G.W. and J.H. thank the Deutsche Forschungsgemeinschaft, DFG, for continuous support during the last 15 years through SFB 303 and 494 for the project of finding a pathway for synthesizing gas-phase HSOH. The Cologne group has been supported by DFG research grant SFB 494 and by special funding from the Ministry of Science of the province of Nordrhein-Westfalen. J.G. thanks the DFG and the Fonds der Chemischen Industrie. E. H. thanks NASA for support of the Ohio State program in laboratory astrophysics.

[1] G. Winnewisser, M. Winnewisser, W. Gordy, *J. Chem. Phys.* **1968**, *49*, 3465 – 3478.
[2] G. Pelz, K. M. T. Yamada, G. Winnewisser, *J. Mol. Spectrosc.* **1993**, *159*, 507 – 520.
[3] P. Helminger, W. C. Bowman, F. C. De Lucia, *J. Mol. Spectrosc.* **1981**, *85*, 120 – 130.
[4] a) H. Wallmeier, W. Kutzelnigg, *J. Am. Chem. Soc.* **1979**, *101*, 2804 – 2814; b) T. J. Lee, N. C. Handy, J. E. Rice, A. C. Scheiner, H. F. Schaefer, *J. Chem. Phys.* **1986**, *85*, 3930 – 3938.

[5] J.-M. Flaud, C. Camy-Peyret, J. W. C. Johns, B. Carli, *J. Chem. Phys.* **1989**, *91*, 1504 – 1510.
[6] J. Hahn, P. Schmidt, K. Reinartz, J. Behrend, G. Winnewisser, K. M. T. Yamada, *Z. Naturforsch. B* **1991**, *46*, 1338 – 1342.
[7] J. Behrend, P. Mittler, G. Winnewisser, K. M. T. Yamada, *J. Mol. Spectrosc.* **1991**, *150*, 99 – 119.
[8] R. R. Smardzewski, M. C. Lin, *J. Chem. Phys.* **1977**, *66*, 3197 – 3204.
[9] M. Iraqi, H. Schwarz, *Chem. Phys. Lett.* **1994**, *221*, 359 – 362.
[10] a) J. R. Shelton, K. E. Davis, *J. Am. Chem. Soc.* **1967**, *89*, 718 – 719; b) E. Block, *J. Am. Chem. Soc.* **1972**, *94*, 642 – 644; c) E. Block, J. O′Conner, *J. Am. Chem. Soc.* **1974**, *96*, 3929 – 3944; d) R. E. Penn, E. Block, L. K. Revell, *J. Am. Chem. Soc.* **1978**, *100*, 3622 – 3623; e) F. A. Davis, R. L. Billmers, *J. Org. Chem.* **1985**, *50*, 2593 – 2595.
[11] A. Königshofen, M. Behnke, M. Hoverath, J. Hahn, *Z. Anorg. Allg. Chem.* **1999**, *625*, 1778 – 1786.
[12] R. Smakman, T. J. De Boer, *Org. Mass Spectrom.* **1970**, *3*, 1561 – 1588.
[13] F. P. Lossing, G. P. Semeluk, *Intern. J. Mass Spectrom. Ion Phys.* **1969**, 2, 408 – 413.
[14] P. De Maria in *"The Chemistry of Sulphenic Acids and their Derivatives"* (Ed.: S. Patai), Wiley, New York, **1990**, p. 293.
[15] See, for example, a) T. Helgaker, J. Gauss, P. Jørgensen, J. Olsen, *J. Chem. Phys.* **1997**, *106*, 6430 – 6440; b) K. L. Bak, J. Gauss, P. Jørgensen, J. Olsen, T. Helgaker, J. F. Stanton, *J. Chem. Phys.* **2001**, *114*, 6548 – 6556.
[16] For recent reviews on coupled-cluster methods, see: a) R. J. Bartlett, J. F. Stanton in *Reviews in Computational Chemistry*, *Vol.5*, (Eds.: K. B. Lipkowitz, D. B. Boyd), VCH, New York, **1994**, p. 65 ff; b) T. J. Lee, G. E. Scuseria in *Quantum Mechanical Electronic Structure Calculations with Chemical Accuracy*, (Ed.: S. R. Langhoff), Kluwer, Dordrecht, **1995**, p. 47 ff; c) R. J. Bartlett in *Modern Electronic Structure Theory*, (Ed.: D. R. Yarkony), World Scientific, Singapore, **1995**, p. 1047 ff; d) J. Gauss in *Encyclopedia of Computational Chemistry*, (Eds.: P. von R. Schleyer, N. L. Allinger, T. Clark, J. Gasteiger, P. A. Kollmann, H. F. Schaefer, P. R. Schreiner), Wiley, New York, **1998**, p. 615 ff.
[17] K. Raghavachari, G. W. Trucks, J. A. Pople, M. Head-Gordon, *Chem. Phys. Letters* **1989**, *157*, 479 – 483 ff.
[18] T. H. Dunning, *J. Chem. Phys.* **1989**, *90*, 1007 – 1023.
[19] J. F. Stanton, J. Gauss, O. Christiansen, *J. Chem. Phys.* **2001**, *114*, 2993 – 2995.
[20] C. Møller, M. S. Plesset, *Phys. Rev.* **1934**, *46*, 618 – 622.
[21] G. D. Purvis, R. J. Bartlett, *J. Chem. Phys.* **1982**, *76*, 1910 – 1918.
[22] K. A. Peterson, T. H. Dunning, *J. Chem. Phys.* **2002**, *118*, 10548 – 10560.
[23] a) A. C. Scheiner, G. E. S. Scuseria, J. E. Rice, T. J. Lee, H. F. Schaefer, *J. Chem. Phys.* **1987**, *87*, 5361 – 5373; b) J. Gauss, J. F. Stanton, R. J. Bartlett, *J. Chem. Phys.* **1991**, *95*, 2623 – 2638; c) T. J. Lee, A. Rendell, *J. Chem. Phys.* **1991**, *94*, 6229 – 6236; d) J. D. Watts, J. Gauss, R. J. Bartlett, *Chem. Phys. Letters* **1992**, *200*, 1 – 7.
[24] I. M. Mills in *Modern Spectroscopy: Modern Research*, (Eds.: K. N. Rao, C. W. Matthews), Academic Press, New York, **1972**, p. 155 ff.
[25] J. Gauss, J. F. Stanton, *Chem. Phys. Letters* **1997**, *276*, 70 – 77.
[26] J. F. Stanton, J. Gauss, *Int. Rev. Phys. Chem.* **2000**, *19*, 61 – 95.
[27] J. F. Stanton, J. Gauss, J. D. Watts, W. J. Lauderdale, R. J. Bartlett, *Int. J. Quantum Chem. Symp.* **1992**, *26*, 879 – 894.
[28] a) J. M. Flaud, C. Camy-Peyret, J. W. C. Johns, B. Carli, *J. Chem. Phys.* **1989**, *91*, 1504 – 1510; b) S. Urban, E. Herbst, P. Mittler, G. Winnewisser, K. M. T. Yamada, *J. Mol. Spectrosc.* **1989**, *137*, 327 – 353.
[29] W. Gordy, R. L. Cook, *Microwave Molecular Spectra. Techniques of Chemistry*, *Volume XVIII*; Wiley, New York, **1984**.
[30] a) G. Winnewisser, *J. Chem. Phys.* **1972**, *56*, 2944 – 2954; b) G. Winnewisser, *J. Chem. Phys.* **1972**, *57*, 1803 – 1804; c) G. Winnewisser, *J. Mol. Spectrosc.* **1972**, *41*, 534 – 547.
[31] H. M. Pickett, *J. Mol. Spectrosc.* **1991**, *148*, 371 – 377.
[32] The theoretically predicted rotational constants A_0, B_0, and C_0 for $H^{34}SOH$ are 201 806.9, 14 998.4, and 14 573.9 MHz (CCSD(T)/cc-pCVQZ calculations with CCSD(T)/cc-pVTZ vibrational corrections).
[33] J. Drabowicz, M. Mikolajczyk, *Synthesis* **1978**, 758 – 759.
[34] M. Winnewisser, H. Lichau, F. Wolf, *J. Mol. Spectrosc.* **2000**, *202*, 155 – 162.
[35] F. Maiwald, F. Lewen, V. Ahrens, M. Beaky, R. Gendriesch, A. N. Koroliev, A. A. Negirev, D. G. Paveljev, B. Vowinkel, G. Winnewisser, *J. Mol. Spectrosc.* **2002**, *202*, 166 – 168.
[36] a) G. Winnewisser, A. F. Krupnov, M. Yu. Tretyakov, M. Liedtke, F. Lewen, A. H. Saleck, R. Schieder, A. P. Shkaev, S. V. Volokhov, *J. Mol. Spectrosc.* **1994**, *165*, 294 – 300; b) G. Winnewisser, *Vib. Spectrosc.* **1995**, *8*, 241 – 253.
[37] R. Gendriesch, F. Lewen, G. Winnewisser, J. Hahn, *J. Mol. Spectrosc.* **2000**, *203*, 205 – 207.
[38] **Note added in proof** (September 9, 2003): Initiated by a seminar at the ETH Zürich presented by one of us (G.W., fall 2001), M. Quack and M. Willeke computed the torsional tunneling splitting for the vibrational ground state of HSOH (M. Quack and M. Willeke, *Helv. Chim. Acta* **2003**, *86*, 1641 – 1653) in good agreement with the present experimental results. We thank Prof. M. Quack (ETH Zürich) for drawing our attention to his results.

Received: May 19, 2003 [F5192]

